24th INTERNATIONAL CONGRESS ON SOUND AND VIBRATION
23–27 July 2017, London

SENSITIVITY ANALYSIS OF THERMOACOUSTIC INSTABILITIES

Francesca Sogaro[1], Peter Schmid[1], Aimee S. Morgans[2]
[1]*Imperial College London, Department of Mathematics, 180 Queen's Gate, London, UK*
[2] *Imperial College London, Mechanical Engineering, Exhibition Road, London, UK*
email: fms14@imperial.ac.uk

Thermoacoustic instability is a phenomenon that occurs in numerous combustion systems, from rockets to land based gas turbines. The resulting acoustic oscillations can result in severe vibrations, thrust oscillations, thermal stresses and mechanical loads that lead to fatigue or even failure. This propensity to instability has been found to occur much more frequently in lean premixed combustion, one of the recent methods used in the gas turbine industry of aeroengines and power gas turbines to reduce NOx emissions. In this work we consider a simplified combustion system, and analyse the sensitivity of its thermoacoustic modes to small changes in the flame and combustor geometry parameters. Such a sensitivity analysis offers insights on how best to change the combustion system so as to "design-out" instability. The simplified combustor is modelled using a low order network representation: linear plane acoustic waves are combined with the appropriate acoustic boundary and flame jump conditions and a linear n-tau flame model. A sensitivity analysis is then performed using adjoint methods, with special focus on the sensitivity of the modes to parameters, such as reflection coefficients and flame model gain and time delay. The gradient information obtained reveals how the thermoacoustic modes of the system respond to changes to the various parameters. The results offer key insights into the behaviour and coupling of different types of modes - for example acoustic modes and so-called "intrinsic" modes associated with the flame model. They also provide insights into the optimal configuration for the design of such combustors.

Keywords: thermo acoustics, intrinsic modes

1. Introduction

The flame-acoustic interaction has received much attention since Rayleigh proposed the feedback mechanism between unsteady heat release fluctuations and pressure fluctuations [1]. The unsteady flame behaviour in the calculation of thermoacoustic modes can be well approximated by a simple linear transfer function like the $n-\tau$ model [2]. Using this model and assuming zero Mach number, [3, 4] the stability of the first acoustic mode of a Rijke tube is shown to alternate between stable and unstable as the time delay of the flame transfer function is increased. Its stability changes approximately when the time delay increases by a factor of π/ω_0 (where ω_0 is the organ pipe mode frequency under consideration). This is equivalent to shifting the phase of the heat release by 180° which translates, according to Rayleigh criterion, into an excitation (or damping) of the mode under consideration. More recent contributions by [5] also perform a sensitivity analysis with an $n-\tau$ model in the zero Mach number limit and show that the time delay has an effect on the stability of the first acoustic mode particularly when the flame is in the first half of the duct [5]. The effect of

the flame element has recently been shown to also give rise to intrinsic flame instabilities [6]. They showed that the flame element not only interacts with the acoustic modes but also causes instabilities without the acoustic feedback mechanism. This can be clearly observed when no acoustic reflection is enforced at the boundaries.

2. Derivation of the wave based model for a Rijke tube

A schematic of the Rijke tube can be seen in figure 1. Early experiments on the system were performed with the tube in its vertical position such that a mean flow induced by convection is established [7]. Turbine combustors are generally oriented horizontally and the mean flow is due to the compressor upstream. The regions upstream and downstream of the flame generally present different mean flow properties due to the mean heat addition of the flame. As a result, the wave equation is to be solved in the two regions separately while interpreting the flame as a jump condition [8].

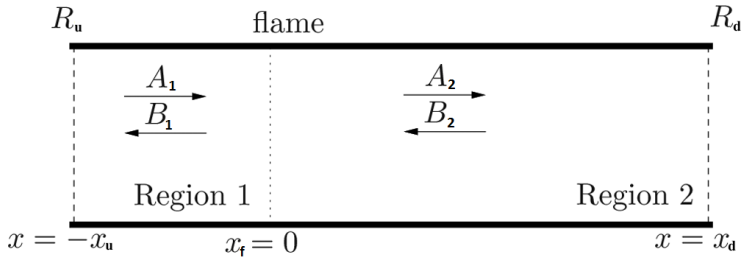

Figure 1: Schematic of the Rijke tube problem

The form of the pressure and velocity fluctuations that satisfy the wave equation are as follows:

$$P_i' = A_i\left(t - \frac{x}{\overline{c_i}+\overline{u_i}}\right) + B_i\left(t + \frac{x}{\overline{c_i}-\overline{u_i}}\right) \tag{1}$$

$$u_i' = \frac{1}{\overline{\rho_i}\overline{c_i}}\left(A_i\left(t - \frac{x}{\overline{c_i}+\overline{u_i}}\right) - B_i\left(t + \frac{x}{\overline{c_i}-\overline{u_i}}\right)\right) \tag{2}$$

where $i = 1,2$ corresponds to the respective sections and the letters A and B represent, respectively, the amplitude of the forward and backward travelling waves. The form of the density fluctuation is the same as for the pressure, but multiplied by a factor of $1/\overline{c_i}^2$. In general an entropy wave is also present as an additional term in the downstream region [9], but in the case of small Mach numbers and open tube ends we can neglect this effect.

To simplify the analysis the wave form of the solution is transformed into the Laplace domain as follows:

$$\hat{P}_i = A_i(s)e^{\left(-s\frac{x}{\overline{c_i}+\overline{u_i}}\right)} + B_i(s)e^{\left(s\frac{x}{\overline{c_i}-\overline{u_i}}\right)} \qquad \hat{u}_i = \frac{1}{\overline{\rho_i}\overline{c_i}}\left(A_i(s)e^{\left(-s\frac{x}{\overline{c_i}+\overline{u_i}}\right)} - B_i(s)e^{\left(s\frac{x}{\overline{c_i}-\overline{u_i}}\right)}\right) \tag{3}$$

In order to complete the system of governing equations, we need boundary conditions at x_u and x_d as well as the jump condition at the flame location x_f. The boundary conditions can assume the form of a transfer function (in the Laplace domain) relating the impinging wave to the reflected one (e.g at the inlet $A_1/B_1 = R_u(s)$ while at the outlet $B_2/A_2 = R_d(s)$). The relations read:

$$R_u B_1(s) e^{\left(s\frac{-x_u}{\overline{c_1}-\overline{u_1}}\right)} = A_1(s) e^{\left(-s\frac{-x_u}{\overline{c_1}+\overline{u_1}}\right)} \qquad R_d A_2(s) e^{\left(-s\frac{x_d}{\overline{c_2}+\overline{u_2}}\right)} = B_2(s) e^{\left(s\frac{x_d}{\overline{c_2}-\overline{u_2}}\right)} \tag{4}$$

$$B_2(s) = R_d A_2(s) e^{\left(-s\frac{2\overline{c_2}x_d}{\overline{c_2}^2-\overline{u_2}^2}\right)} \qquad A_1(s) = R_u B_1(s) e^{\left(-s\frac{2\overline{c_1}x_u}{\overline{c_1}^2-\overline{u_1}^2}\right)}$$

The exponents represent the time delay for a wave to travel along the section length and back, and hence we can call them $\tau_u = \frac{2\overline{c_1}x_u}{\overline{c_1}^2-\overline{u_1}^2}$ and $\tau_d = \frac{2\overline{c_2}x_d}{\overline{c_2}^2-\overline{u_2}^2}$.

The dimension of an air-methane flame under standard conditions is significantly smaller than the wavelength of the acoustic wave [10]. Hence the flame front, seen by the acoustic wave, can be treated as a planar discontinuity and can be referred to as compact [10]. The flame jump conditions are derived by imposing the governing equations across the flame [8] and read as follows, where $[\![\cdot]\!] = (\cdot_{x_f^+} - \cdot_{x_f^-})$:

$$[\![P]\!] + \rho_1 u_1 [\![u]\!] = 0 \tag{5}$$

$$\frac{\gamma}{\gamma-1}[\![Pu]\!] + \frac{1}{2}\rho_1 u_1 [\![u^2]\!] = Q/A \tag{6}$$

$$\tag{7}$$

After the linearisation, the jump conditions for the fluctuating quantities are:

$$[\![P']\!] + \overline{\rho_1}\,\overline{u_1}[\![u']\!] + (\overline{\rho_1}u_1' + \rho_1'\overline{u_1})[\![\overline{u}]\!] = 0 \tag{8}$$

$$\left(\frac{\gamma}{\gamma-1}\right)\left([\![\overline{P}u']\!] + [\![\overline{u}P']\!]\right) + \frac{1}{2}\left(\overline{\rho_1}\,\overline{u_1}[\![2\overline{u}u']\!] + \overline{\rho_1}u_1'[\![\overline{u}^2]\!] + \rho_1'\overline{u_1}[\![\overline{u}^2]\!]\right) = Q'/A$$

By implementing the jump conditions for the position of the flame at $x_f = 0$, we can recast the system in matrix form (the expression for the coefficients can be found in the Appendix A:

$$\begin{bmatrix} X_{11} - Y_{11}R_u e^{-s\tau_u} & X_{12} - Y_{12}R_d e^{-s\tau_d} \\ X_{21} - Y_{21}R_u e^{-s\tau_u} & X_{22} - Y_{22}R_d e^{-s\tau_d} \end{bmatrix} \begin{bmatrix} B_1(s) \\ A_2(s) \end{bmatrix} = \begin{bmatrix} 0 \\ \hat{Q}(s)/(\overline{c_1}A) \end{bmatrix} \tag{9}$$

At this stage the only unknown left to be determined is the form of the fluctuating heat release rate $\hat{Q}$. In the Laplace domain this is given by the flame transfer function relating the impinging velocity fluctuation (which transports the reactants) to the mean heat release rate. In this work we use the $n-\tau$ model [2], defined as (at $x = 0$):

$$H(s) = \frac{\hat{Q}(s)}{\overline{Q}}\frac{\overline{u_1}}{\hat{u_1}(s)} = n_f e^{-s\tau_f} \tag{10}$$

$$\hat{Q}(s) = \frac{n_f\overline{Q}}{\overline{u_1}}\frac{B(s)}{\overline{\rho_1}c_1}(R_u e^{-s\tau_u} - 1)e^{-s\tau_f}$$

For simplicity we rename $m = \frac{n_f\overline{Q}}{A\overline{\rho_1}c_1u_1}$. Substituting this expression into the above matrix and rearranging, we can obtain a system in the form $\mathbf{Mx} = 0$ where $\mathbf{x} = [B_1(s), A_2(s)]^T$.

$$\begin{bmatrix} X_{11} - Y_{11}R_u e^{-s\tau_u} & X_{12} - Y_{12}R_d e^{-s\tau_d} \\ X_{21} - Y_{21}R_u e^{-s\tau_u} - me^{-s\tau_f}(R_u e^{-s\tau_u} - 1) & X_{22} - Y_{22}R_d e^{-s\tau_d} \end{bmatrix} \begin{bmatrix} B_1(s) \\ A_2(s) \end{bmatrix} = \begin{bmatrix} 0 \\ 0 \end{bmatrix} \tag{11}$$

Once the system is in this form, the dispersion relation is obtained by setting the determinant of the matrix $\mathbf{M}$ to zero. The Laplace variable s represents the complex eigenfrequency of the system ($s = \sigma + i\omega$). Frequently it will be simply referred to as the 'eigenvalue' but this should not be confused with the eigenvalues of the matrix $\mathbf{M}$.

3. Adjoint analysis

The use of sensitivity analysis in design is an active area of research but has only recently been applied to thermoacoustic systems. In this section we derive the method used in this work but the reader is referred to reviews and introductions from authors like [11, 12] for more details on the derivations.

3.1 Derivation of a general sensitivity equation

We consider the system given by $\mathbf{Mq} = \mathbf{f}$ where $\mathbf{M}(s,p)$, $\mathbf{q}$, $\mathbf{f}(s,p) \in \mathbb{C}$. The variable p represents a set of parameters and boundary conditions of the problem ($p = (\tau_f, x_u, x_d, x_f, R_u, R_d, l, ...)$). The variable s is defined as before. In sensitivity studies we are interested in identifying the variation of the eigenvalues of the system with respect to a slight variation in the parameters p [13], this was also called base sensitivity by [14]. Using Lagrange multipliers we can derive an expression for the sensitivity of the i^{th} eigenvalue s_i to changes in the parameter or boundary conditions, i.e. $\partial s_i/\partial p$. We now define the scalar cost functional $J = \Re(s(p))$ as any real scalar objective that we want to minimise, for example the real part of the least stable eigenvalue. We can reformulate our constrained optimization problem as an unconstrained one using the Lagrange multiplier approach.

$$\mathscr{L} = J - \langle \mathbf{a}, \mathbf{Mq} - \mathbf{f} \rangle = J - \mathbf{a}^*(\mathbf{Mq} - \mathbf{f}) \tag{12}$$

where the costate is $\mathbf{a} \in \mathbb{C}$. An appropriate inner product $\langle , \rangle$ for the complex case has been applied and the $*$ symbol denotes the complex conjugate transpose.

The variable $\delta\mathscr{L}$ is obtained by a first variation, and the optimisation procedure requires $\delta\mathscr{L} = 0$ for every $\delta\mathbf{a}$, $\delta\mathbf{q}$, δp and $\delta\mathbf{f}$. This leads to a set of equations that has to be satisfied to optimise the system.

$$\delta\mathscr{L} = \left\langle \frac{\partial \mathscr{L}}{\partial \boldsymbol{a}}, \delta\boldsymbol{a} \right\rangle + \left\langle \frac{\partial \mathscr{L}}{\partial \boldsymbol{q}}, \delta\boldsymbol{q} \right\rangle + \left\langle \frac{\partial \mathscr{L}}{\partial \boldsymbol{f}}, \delta\boldsymbol{f} \right\rangle + \left\langle \frac{\partial \mathscr{L}}{\partial p}, \delta p \right\rangle \tag{13}$$

The first term (differentiation with respect to the costate) retrieves the governing equations, the differential with respect to the state variable gives the adjoint equation, and finally the equation for the sensitivity is obtained by differentiating with respect to the design parameter of choice. The differentiation with respect to the forcing $\boldsymbol{f}$ is not treated in this work.

$$\begin{aligned}
\left\langle \frac{\partial \mathscr{L}}{\partial \boldsymbol{a}}, \delta\boldsymbol{a} \right\rangle &= (\boldsymbol{Mq} - \boldsymbol{f})^* \delta\boldsymbol{a} \\
\left\langle \frac{\partial \mathscr{L}}{\partial \boldsymbol{q}}, \delta\boldsymbol{q} \right\rangle &= -(\boldsymbol{M}^*\boldsymbol{a})^* \delta\boldsymbol{q} \\
\left\langle \frac{\partial \mathscr{L}}{\partial p}, \delta p \right\rangle &= \frac{\partial J}{\partial p}\delta p - \left(\boldsymbol{a}^* \frac{\partial \boldsymbol{M}}{\partial p}\boldsymbol{q} - \boldsymbol{a}^* \frac{\partial \boldsymbol{f}}{\partial p} \right) \delta p
\end{aligned} \tag{14}$$

To obtain an expression for the sensitivity to the design parameters all three conditions must be

solved simultaneously. Hence the system is

$$\begin{aligned} &\frac{\partial J}{\partial p} = \boldsymbol{a}^* \frac{\partial \boldsymbol{M}}{\partial p}\boldsymbol{q} - \boldsymbol{a}^* \frac{\partial \boldsymbol{f}}{\partial p} \\ &\boldsymbol{M}\boldsymbol{q} - \boldsymbol{f} = \boldsymbol{0} \\ &\boldsymbol{M}^*\boldsymbol{a} = \boldsymbol{0} \end{aligned} \tag{15}$$

At this point it is important to note that the matrix $\mathbf{M}$ is a function of both p and the eigenvalue s, which is in turn a function of p. Furthermore, both the cost functional J and the vector $\mathbf{f}$ can also be a function of s. In the present thermoacoustic system there is no forcing (**f=0**) and we are interested in the behaviour of the eigenvalues with $J = 0$. We then obtain:

$$\frac{\partial s_i}{\partial p} = \frac{\boldsymbol{a}^* \frac{\partial \boldsymbol{M}}{\partial p}\boldsymbol{q}}{\boldsymbol{a}^* \frac{\partial \boldsymbol{M}}{\partial s}\boldsymbol{q}} \tag{16}$$

This is a relatively simple expression that can provide insightful information on the behaviour of the system's modes in response to changes in parameters.

4. Results

A preliminary analysis for a case of zero Mach number and zero mean heat addition provides an insight on the behaviour of both the acoustic and intrinsic modes. The following special cases of analytical solutions can be obtained when setting the determinant of the system (11) to zero:

- $m = 0$: This is obtained with a zero gain in the $n-\tau$ model ($n_f = 0$) and recovers simple organ pipe acoustic modes

$$\begin{cases} \omega = k\pi\bar{c}/(2l) \\ \sigma = -\frac{\bar{c}}{2l}\ln\left(\frac{1}{R_u R_d(-1)^k}\right) \text{ with } k \text{ such that } (R_u R_d(-1)^k > 0)\ , k \in \mathbb{Z} \end{cases}$$

- $R_u = R_d = 0$: This case represents an anechoic situation. This situation eliminates the organ pipe modes and highlights the presence of intrinsic modes. The form of the solution is

$$\begin{cases} \omega = \frac{nk}{\tau_f} \\ \sigma = -\frac{1}{\tau_f}\ln\left(\frac{-2}{(-1)^k m}\right) \text{ with } k \text{ such that } (m(-1)^k < 0)\ , k \in \mathbb{Z} \end{cases}$$

- $R_u = R_d$ and $\tau_u = \tau_d$: for example a Rijke tube with closed-ends and the flame placed in the middle. This symmetric configuration allows us to recover the intrinsic and acoustic solutions without allowing them to interact.

The present study focusses mainly on the effect of the location of the flame and the time delay used in the $n-\tau$ model. In particular, we investigate how, by placing the flame in different locations of a Rijke tube with closed ends, the behaviour of the modes of the system changes. Figure 2 shows the effect of changing the flame position on the evolution of the eigenvalues in the complex plane. The plots have been chosen with $x_f \in \{0.5, 0.35, 0.25\}$. The symmetric configuration (figure 2a), as derived analytically, shows non-interacting intrinsic and acoustic modes. Shifting the flame upstream (figure 2b) drastically changes the behaviour of the modes as the $n-\tau$ model time delay is changed. The acoustic modes describe ellipses while the intrinsic ones also oscillate from their $1/\tau_f$ trajectories. Most importantly, when the intrinsic modes enter one of the acoustics orbits they replace the mode and force it to move to a lower frequency. These interactions differ depending on the modes, it can be seen that the third organ pipe mode of figure 2b remains unaffected by the intrinsic

modes. This can be better explained by looking at figure 2c, when the flame is at $x_f = 0.25$. We see that the second and 4th acoustic mode recover the 'classical' form of perfect organ pipe modes, suggesting that a feedback mechanism cannot be established between the flame and these acoustic modes. This highlights the importance of the flame position, in particular, as it governs the magnitude of the upstream and downstream time delays and therefore the phase of the reflected waves from the boundaries. It is argued that if the reflected waves interact destructively at the flame location (e.g. symmetric case) the interaction between acoustic and intrinsic modes can be removed.

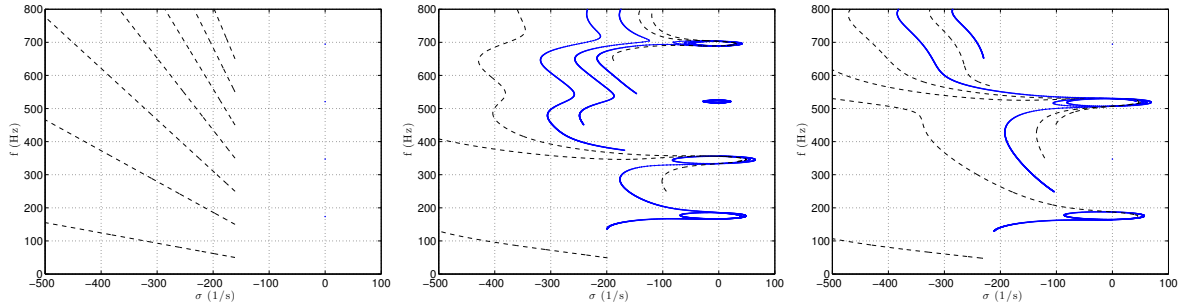

(a) $x_f = 0.50$ (b) $x_f = 0.35$ (c) $x_f = 0.25$

Figure 2: Acoustic (blue) and Intrinsic modes (black) in the complex plane at the time delay is increased in the range [1-10]ms for the flame at location x_f =0.25, 0.35, 0.5

Sensitivity analysis can provide further information on this behaviour. The sensitivity presented here has been performed with the location of the flame gradually changing within the range $x_f = [0.4, 0.5]$. This allows us to study the behaviour of the first acoustic mode as we perturb the symmetric configuration. Figure 3a shows the evolution of the interaction. The acoustic mode draws increasingly larger ellipses until a swap with the intrinsic mode occurs. Figure 3b, representing the evolution of the frequencies, allows us to better detect when this interaction occurs, around $\tau_f = 7.5 - 8$ms. The sensitivities with respect to the upstream reflection coefficient (R_u), downstream reflection coefficient (R_d), the flame position (x_f) and cut-off frequency (τ_1) are shown in figures 3c,d,e,f respectively. Sensitivity with respect to R_u highlights very clearly that the intrinsic modes are not particularly affected by this design parameter. In the neighbourhood of a swapping condition their sensitivity increases and, jumps to values of the acoustic one when the swap occurs. The downstream reflection coefficient (R_d) is similar to the upstream one in both magnitude and behaviour. Sensitivities to the flame position are an order of magnitude larger than the previous ones, however the overall behaviour of a peak in sensitivity in the neighbourhood of the swap is also observed here. The results clearly show that the swap in modes is reflected also in the sensitivities. In particular the modes show higher sensitivity in the regions when the swaps occur.

5. Conclusions

The main finding is the occurrence of an interaction between the intrinsic and acoustic modes. This interaction generally occurs when the time delay of the intrinsic modes is sufficiently large such that the $-1/\tau_f$ term in front of the expression for the growth rates of the intrinsic modes assumes values similar to those of the acoustic modes. Secondly, the location of the flame determines the susceptibility of the acoustic modes to actually interact with the intrinsic ones. If the location is such that the acoustic velocity perturbation is small, its mode will not be affected by a change in time delay. Vice versa, the farther from these locations, the more the acoustic modes will be affected. This is easily observed by plotting the behaviour of the modes in the complex plane (figure 2). We argue that it is important to take into account the interaction between the acoustic and intrinsic modes in order to fully understand the sensitivity analysis. In particular, higher sensitivity has been observed to correspond and highlight the location and time delays at which these interactions occur.

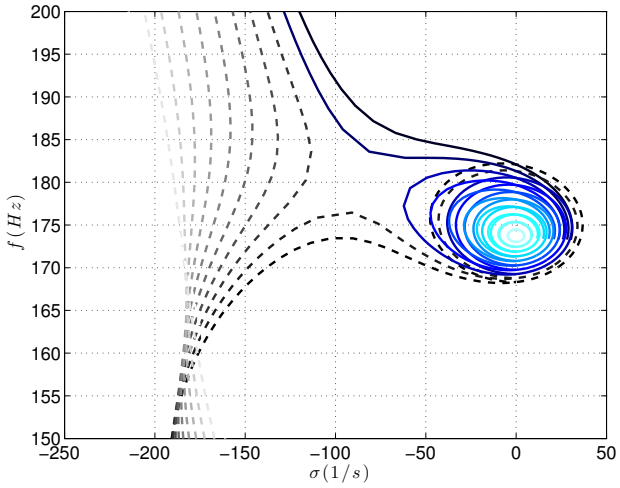

(a)
Complex plane

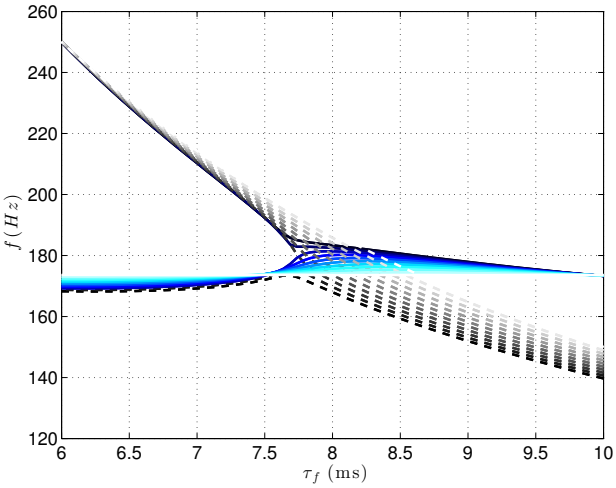

(b)
Frequencies

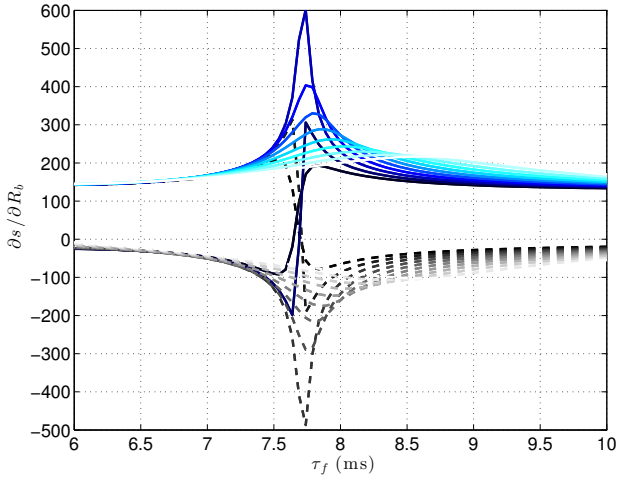

(c) Sensitivity with respect to R_u $6 < \tau_f < 10$ms

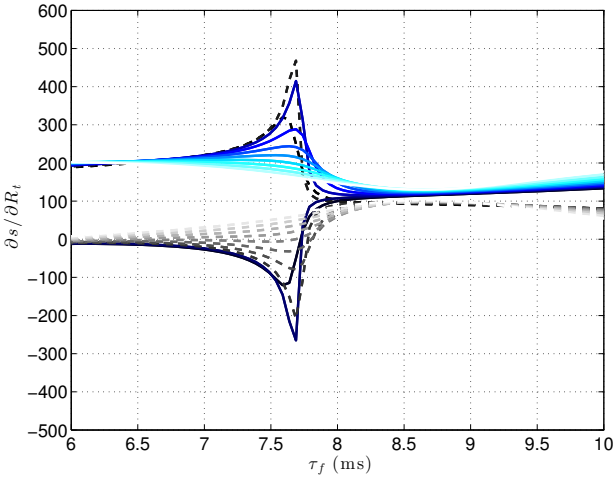

(d) Sensitivity with respect to R_d $6 < \tau_f < 10$ms

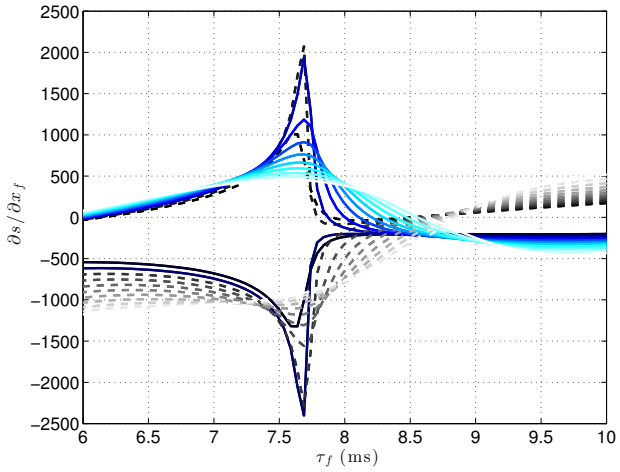

(e) Sensitivity with respect to x_f $6 < \tau_f < 10$ms

Figure 3: Complex plane (a) and frequency plot (b) of the interaction of the first acoustic mode with the intrinsic one. Plots are enlarged in the region where the time delay τ_f is in the range {6-10}ms and the flame position is changed from its symmetric configuration to 0.4 towards the inlet. Sensitivities with respect to the upstream reflection coefficient (c), the downstream reflection coefficient (d) and the flame position (e) are also shown.

The investigation presented here constitutes a preliminary analysis on the interaction that intrinsic and acoustic modes can present. Further investigations are necessary to fully understand the nature of this interaction. However, the importance of the flame location has been identified from the sensitivity analysis to be a major player in the interaction.

REFERENCES

1. Rayleigh, J. W. S., *The theory of sound*, Dover Publications (1945).
2. Crocco, L. Research on combustion instability in liquid propellant rockets, *Symposium (International) on Combustion*, **12** (1), 85–99, (1969).
3. Morgans, A. S. and Dowling, A. P. Model-based control of combustion instabilities, *Journal of Sound and Vibration*, **299** (1-2), 261–282, (2007).
4. Dowling, A. P. and Morgans, A. S. Feedback control of combustion oscillations, *Annual Review of Fluid Mechanics*, **37**, 151–82, (2005).
5. Aguilar, J. G., Magri, L. and Juniper, M. P. Adjoint-based sensitivity analysis of low order thermoacoustic networks using a wave-based approach, *TUM*, pp. 1–11, (2011).
6. Hoeijmakers, M., Kornilov, V., Lopez Arteaga, I., de Goey, P. and Nijmeijer, H. Intrinsic instability of flame-acoustic coupling, *Combustion and Flame*, **161** (11), 2860–2867, (2014).
7. Rijke, P. A new method of causing vibration of the air contained in a tube open at both ends, *Phil. Magazine*, **17**, 419, (1895).
8. Dowling, A. P. Nonlinear self-excited oscillations of a ducted flame, *J. Fluid Mech.*, **346**, 271–290, (1997).
9. Goh, C. S. and Morgans, A. S. The Influence of Entropy Waves on the Thermoacoustic Stability of a Model Combustor, *Combustion Science and Technology*, (March), 120816123400009, (2013).
10. Lieuwen, T. C. and Yang, V., *Combustion instabilities in gas turbine engines. Operational experience, fundamental mechanisms and modelling*, AIAA, vol 210 edn. (2005).
11. Cossu, C. An Introduction to Optimal Control, *Applied Mechanics Reviews*, **66** (March), 021001, (2014).
12. Giles, M. B. and Pierce, N. A. An introduction to the adjoint approach to design, *Flow, Turbulence and Combustion*, **65** (3-4), 393–415, (2000).
13. Meneghello, G., Schmid, P. J. and Huerre, P. Receptivity and sensitivity of the leading-edge boundary layer of a swept wing, *J. Fluid Mech.*, **775**, R1, (2015).
14. Magri, L. and Juniper, M. P. Global modes, receptivity, and sensitivity analysis of diffusion flames coupled with duct acoustics, *Journal of Fluid Mechanics*, **752** (2005), 237–265, (2014).

Appendix A.

Coefficients of the matrix **M**

$$
\begin{aligned}
Y11 &= 1-\overline{M_1}\left(\frac{\overline{u_2}}{\overline{u_1}}-2\right)-\overline{M_1}^2\left(\frac{\overline{u_2}}{\overline{u_1}}-1\right) \\
Y12 &= \overline{M_2}-1 \\
Y21 &= \frac{1+\overline{M_1}\gamma}{\gamma-1}+\overline{M_1}^2-0.5\overline{M_1}^2(1+\overline{M_1})\left(\left(\frac{\overline{u_2}}{\overline{u_1}}\right)^2-1\right) \\
Y22 &= \frac{c_2}{c_1}\left(\frac{1-\overline{M_2}\gamma}{\gamma-1}+\overline{M_2}^2\right)
\end{aligned}
\qquad
\begin{aligned}
X11 &= -1-\overline{M_1}\left(\frac{\overline{u_2}}{\overline{u_1}}-2\right)+\overline{M_1}^2\left(\frac{\overline{u_2}}{\overline{u_1}}-1\right) \\
X12 &= \overline{M_2}+1 \\
X21 &= \frac{1-\overline{M_1}\gamma}{\gamma-1}+\overline{M_1}^2-0.5\overline{M_1}^2(1-\overline{M_1})\left(\left(\frac{\overline{u_2}}{\overline{u_1}}\right)^2-1\right) \\
X22 &= \frac{c_2}{c_1}\left(\frac{1+\overline{M_2}\gamma}{\gamma-1}+\overline{M_2}^2\right)
\end{aligned}
\tag{17}
$$